Engineering Fracture Mechanics 253 (2021) 107906

Contents lists available at ScienceDirect

Engineering Fracture Mechanics

journal homepage: www.elsevier.com/locate/engfracmech

Hydrogen embrittlement testing procedure for the analysis of structural steels with Small Punch Tests using notched specimens

G. Álvarez *, A. Zafra, F.J. Belzunce, C. Rodríguez

SIMUMECAMAT research group, University of Oviedo, Edificio Departamental Oeste, Bloque 7, Campus Universitario, 33203 Gijón, Asturias

ARTICLE INFO

Keywords:
Hydrogen embrittlement
Small Punch Tests
CTOD
Notched specimens
Structural steels

ABSTRACT

The influence of hydrogen on the mechanical properties of three structural steels has been evaluated. A testing procedure based on the Small Punch Test with notched specimens was used to measure hydrogen embrittlement. Two pre-charging methods were applied to introduce hydrogen in the samples. The first method used gaseous hydrogen in a high-pressure reactor at 19.5 MPa and 450 °C for 21 h. The second involved cathodic charging from 2 M $H_2SO_4 + As_2O_3$ electrolyte with a current density of 2 mA/cm^2. The results obtained in the Small Punch Tests were compared with those obtained using standard fracture tests. The hydrogen embrittlement behaviour of the different steels, with special attention to the effect of their chemical compositions and microstructures, were compared. The embrittlement indexes obtained with Small Punch Tests are lower than those obtained with standard tests. The low thickness and lower stress triaxiality of the Small Punch Test specimens explains this result. Regardless of the test method used, hydrogen embrittlement grows with the strength of the analysed steel.

1. Introduction

Nowadays the excessive consumption of raw materials for energy production is a controversial environmental issue. There is growing acceptance of hydrogen as one of the best ways to store the energy obtained from renewable resources to battle against climate change [1]. Hydrogen may be the energy vector that replaces fossil fuels; it could also be used in different industrial processes. A great increase in the use of hydrogen is expected in the near future, and facilities for the storage and transportation of hydrogen will proliferate.

On the other hand, the strength of steel industrial components in contact with hydrogen decreases due to hydrogen embrittlement. This embrittlement increases as the strength of the steel increases; it is largely dependent on the microstructure of the steel. For instance, hydrogen embrittlement has been reported in the heat affected zones of welds due to grain coarsening and microstructural modifications of the steel [2-4]. In certain processes and techniques, such as electroplating or cathodic protection, hydrogen is generated and embrittlement can be a serious risk. For all these reasons, the evaluation of hydrogen embrittlement is a critical issue that deserves in depth research studies.

The slow rate tension test (SSRT) is the most common test to evaluate the effect of hydrogen on steel [5-9]. The embrittlement index normally employed in this test is based on the reduction of the fracture area. It is usually complemented by fractographic images which expose some signs of embrittlement. However, these are destructive tests that require a significant amount of material to machine the

* Corresponding author.
E-mail address: alvarezdguillermo@uniovi.es (G. Álvarez).

https://doi.org/10.1016/j.engfracmech.2021.107906
Received 8 June 2021; Received in revised form 1 July 2021; Accepted 16 July 2021
Available online 22 July 2021

test samples. Therefore, in order to monitor components under working conditions without damaging their structural integrity, miniature samples are the best option.

The Small Punch Test (SPT) was developed to evaluate the evolution of the mechanical properties of steels used in nuclear industry under working conditions [10]. In situations where hydrogen is continuously entering steel, there is a similar problem, and degradation of its mechanical properties can be continuously monitored throughout its service life. Various authors have applied the SPT to observe the decline of the mechanical properties of steel and to measure hydrogen embrittlement [11-16], but the most appropriate test procedure has yet to be defined.

Different studies have shown how hydrogen diffuses in steel microstructures, accumulating ahead of notches or cracks where hydrostatic stresses produce a slightly expanded local lattice[17-19]. This research uses standard fracture toughness specimens (cracked samples) and SPT samples with a longitudinal notch [20,21] to increase the hydrostatic stresses and to promote hydrogen embrittlement.

There are two basic techniques to generate hydrogen and to introduce it into steels, through high-pressure hydrogen gas [22-27] and by cathodic charging from an aqueous solution [28-33]. Both methods were used in this paper, followed by mechanical tests on pre-charged specimens in air at room temperature.

An important parameter in these tests is hydrogen diffusivity, whose value depends on the steel microstructure. It changes with vacancy and dislocation densities, strain fields, grain and other internal boundaries, precipitates, inclusions, etc. [33-36]. Permeation tests are usually used to determine the hydrogen diffusivity coefficient (D_{eff}) [37-40]. This parameter is critical to understand why some steels give higher embrittlement indexes than others and how test duration influences the mechanical behaviour of different steels.

The aim of this paper is to evaluate the susceptibility of different steels to hydrogen embrittlement by means of the SPT. The results given by the newly developed SPT method were compared with those of standard fracture toughness tests. In both cases the effects of hydrogen on the behaviour of the material was expressed in function of the decay of fracture toughness and quantified by the Hydrogen Embrittlement Index (HEI) defined as:

$$HEI_X(\%) = \frac{X - X_H}{X} \hat{\mathrm{A}} \cdot 100 \tag{1}$$

where X_H and X are the measured toughness parameter evaluated with and without hydrogen, respectively. The HEI is expressed as a percentage from 0 to 100. At 0%, hydrogen has no influence on the toughness of the material. At 100% the hydrogen embrittlement weakens steel toughness to zero.

2. Materials and methods

2.1. Materials

Three structural steels were used in this research. The steels were selected because they are used in general structural applications and sometimes in hydrogen-rich environments. The first one is a common S355 structural carbon steel which is an economical option when the applied external loads are not high. The second one, H8, is a quenched and tempered alloyed steel used in naval applications in which hydrogen can enter from the salted aqueous medium. The third, WM, is the weld metal of a real CrMoV welded joint after a low temperature post-weld heat treatment, usually used in the manufacturing of pressure vessels and pipes dealing with hydrogen rich gases. Table 1 and Fig. 1 show the chemical composition and the general microstructure of the three steels, respectively. The S355 steel has a ferrite-pearlite microstructure (Fig. 1.a,b), whereas H8 and WM have tempered bainitic-martensitic microstructures (Fig. 1.c,d,e, f).

Table 2 shows the Brinell hardness (*HB*) and the tensile properties (yield stress, σ_{YS}, ultimate strength, σ_u, elongation, *e,* and reduction in area, *RA)* of the steels. Tensile properties were obtained in accordance with the UNE-EN ISO 6892–1 standard [41]:

2.2. Hydrogen pre-charging methods and permeation tests

Two pre-charging methods were used to analyse the effect of internal hydrogen on the mechanical behaviour of steels: gaseous and cathodic charging.

Gaseous pre-charging was carried out in an autoclave, using the same conditions as those employed by Peral et al. [18]: 19.5 MPa of pressure at 450 °C for 21 h (saturated condition). Charging temperature was limited to avoid hydrogen attack. In order to avoid hydrogen egress, after the pre-charging process the specimens were stored in liquid nitrogen until the beginning of the mechanical tests.

Table 1
Chemical composition (% by weight).

Steel	C	Mn	Si	Cr	Cu	Ni	Mo	V
S355	0.13	0.8	0.26	1.58	0.27	0.25	0.05	0.00
H8	0.15	0.25	0.25	1.58	0.13	3.05	0.55	0.05
WM	0.08	0.04	1.08	2.28	–	0.03	0.93	0.24

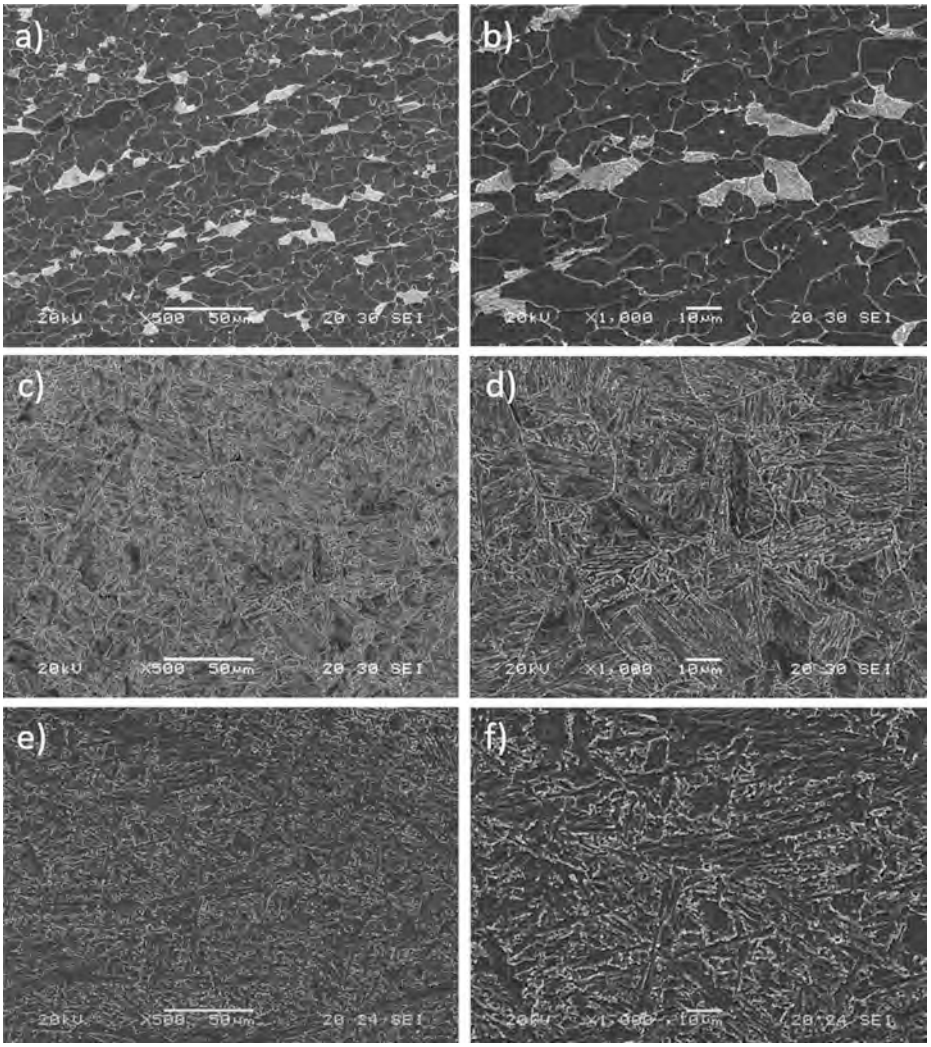

Fig. 1. Microstructure of the steels: a) S355, ×500; b) S355, ×1000; c) H8, ×500; d) H8, ×1000; e) WM, ×500; f) WM, ×1000.

Table 2
Hardness and tensile properties (mean ± standard deviation).

Steel	Hardness	Tensile			
	HB	σ_{YS}(MPa)	σ_u (MPa)	*e*(%)	*RA*(%)
S355	145 ± 3	386 ± 1	472 ± 2	32 ± 0.14	77 ± 1
H8	285 ± 4	790 ± 8	857 ± 10	21 ± 0.51	68 ± 2
WM	360 ± 9	1019 ± 21	1120 ± 1	17 ± 0.11	57 ± 1

Table 3
Initial (immediately after pre-charging) and final (after extended period at RT) hydrogen concentration after pre-charging.

Steel	Gaseous pre-charge (wppm)		Electrolytic pre-charge (wppm)		C_T (wppm)
	C_{H0}	C_{Hdiff}	C_{H0}	C_{Hdiff}	
S355	0.63	0.18	0.55	0.10	0.45
H8	1.30	0.70	2.20	1.60	0.60
WM	2.20	1.10	5.20	4.10	1.10

Cathodic pre-charge was applied according to the procedure detailed in [42]. A 2 M H_2SO_4 + 0.25 g/l As_2O_3 (pH ≈ 1) electrolyte under a current density of 2 mA/cm^2 applied for 4 h was used to introduce the hydrogen in the steel samples. The selection of these parameters is discussed in [42].

The initial hydrogen concentration (C_{H0}) was measured with a LECO DH603 hydrogen analyser on appropriated samples depending on the pre-charging method: pins with a length of 30 mm and 10 mm diameter (≈ 20 g) for gaseous pre-charging and 50x50x1 mm^3 samples for cathodic pre-charging. Table 3 shows the values of hydrogen concentration measured in the three steels for the two hydrogen pre-charging methodologies. Table 3 also shows the strongly trapped hydrogen or residual hydrogen (C_T) present in each steel obtained by means of RT desorption tests. Some pre-charged samples were exposed to air at room temperature for different time intervals, after which, the hydrogen concentration in the samples was measured with the LECO analyser. The concentration of the strongly trapped hydrogen, C_T, was determined as the hydrogen remaining in the sample after an extended period of time (1 month). This value is assumed to be constant regardless of which pre-charging technique is used. The difference between C_T and the initial hydrogen concentration, C_{H0}, is the diffusible hydrogen, C_{Hdiff}, also shown in the Table 3.

It is worth noting that C_{Hdiff} depends on the pre-charging method and also on the steel. The largest growth corresponds to the cathodic pre-charge, except with S355, for which both charging methods gave nearly the same result (as seen in Table 3). Initial and residual hydrogen concentrations increase with the hardness and with the strength of the steel as these properties are closely related to the density of microstructural hydrogen traps. The relatively low hydrogen concentration measured after gaseous pre-charging is partly due to hydrogen egress between the end of the pre-charge and the moment when the samples can be extracted from the reactor (after pre-charging 1 h cooling period is necessary before the autoclave can be opened).

In order to obtain information about the hydrogen diffusion behaviour of the three steels, permeation tests were also carried out. This kind of test uses the same electrolyte as in the cathodic pre-charge. These tests were performed at room temperature using the setup and procedure explained in Álvarez et al. [43]. The evolution of the anodic current density until reaching a steady-state value, i_{ss} (μA.m^{-2}) was measured to determine the diffusion coefficient, D_{eff} (m^2/s), using Expression (2) following the ASTM G148 standard [44].

$$D_{eff} = \frac{d^2}{6t_{0.63}} \tag{2}$$

where d (m) is the specimen thickness, and $t_{0.63}$ (s) is the lag time defined as the elapsed time at $\frac{i_i}{i_{ss}} = 0.63$ (see Fig. 2).

Fig. 2 shows the normalized permeation curves obtained with the three steels. The higher hydrogen diffusivity of the S355 steel is very clear. S355 steel needs only a few minutes to reach the steady state current density (i_{ss}), while H8 steel needs nearly two hours and WM more than eight hours. Table 4 shows the D_{eff} values obtained with the three steels.

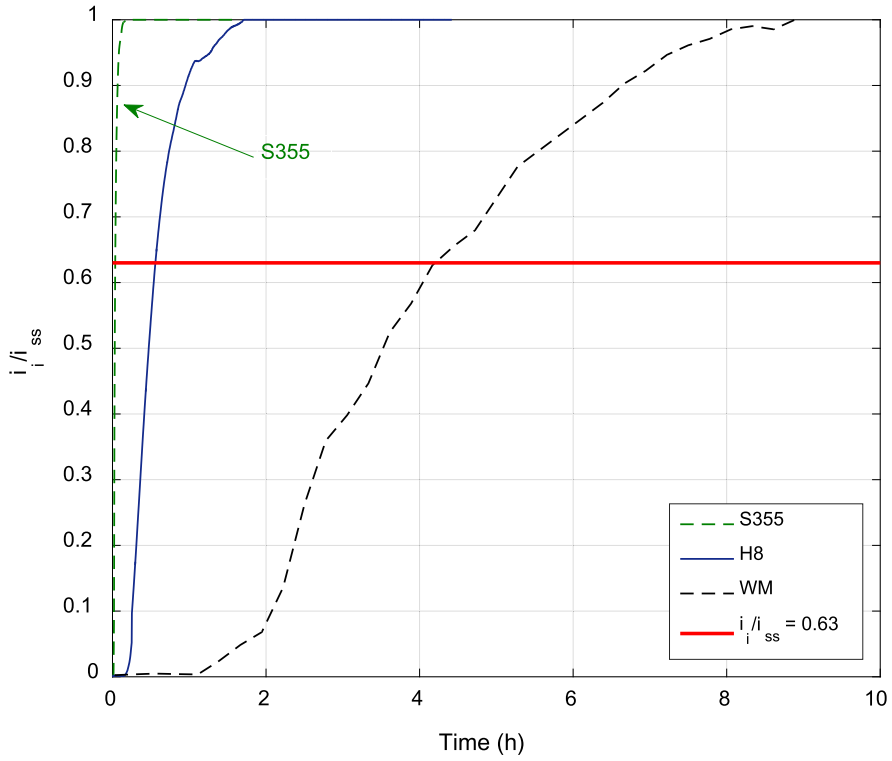

Fig. 2. Permeation test curve.

3. Hydrogen embrittlement analysis

3.1. Standard fracture toughness tests

Standard fracture toughness tests were carried out using single edge notch bend specimens, SEN(B), with width, $W = 17.5$ mm, thickness, $B = 10$ mm, length $L = 80$ mm and an initial notch length, $a_0 = 4$ mm. In accordance with the ASTM E1820 standard [45], the specimens were fatigue pre-cracked ($R = 0.1$) until obtaining a crack length-to-width relation of$a/W = 0.5$. Afterwards, the specimens were side-grooved until reaching a final net-thickness, $B_N = 7.3 \pm 0.05$ mm, except with the WM steel, for which this was not necessary because of its brittleness.

Fracture toughness tests were carried out on non-charged specimens under a load line displacement (*LLD*) rate of 0.1 mm/min. Because the embrittlement effect of hydrogen increases as the test rate decreases [19], hydrogen pre-charged specimens were tested under an *LLD* rate 100 times lower (0.001 mm/min), which approaches the minimum displacement rate allowed by the testing machine employed in this work, as to maximize hydrogen embrittlement.

Crack growth in the course of the tests was determined by means of the compliance method. The value of J obtained in each unload-reload sequence was determined as the sum of its elastic and plastic components. The former was calculated from the stress intensity factor, K, and the latter was obtained by integrating the area below the Load-*LLD* curve, always following the procedure described in the ASTM E1820 standard [45]. The $J_{0.2/BL}$ parameter or J_{Ic} was used to assess the fracture toughness for the onset of crack growth.

Fig. 3 shows the effect of gaseous pre-charged hydrogen on the $J-R$ curves of the three analysed steels. In the case of S355 and H8 steels, the hydrogen embrittlement effect on the $J-R$ curve can be clearly seen. On the other hand, the brittleness of the WM steel made it impossible to obtain a $J-R$ curve. Nevertheless, the effect of hydrogen can be seen in this case on the load-*CMOD* curves presented in Fig. 3.c. In this steel the stress intensity factor for the onset of crack propagation, K_{Ic}, was calculated.

The J_{Ic} values obtained for all the steels and testing conditions are shown in Table 5. It is worth noting the large decrease that the presence of internal hydrogen produces on the fracture toughness of all the analysed steels, but especially in H8, for which a hydrogen embrittlement index, HEI, greater than 90% was measured. WM has a lower HEI, 64%, although it is the most brittle of the three steels in the presence of hydrogen (8 kJ/m^2).

The principal fracture micromechanisms observed on the failed surfaces of all these specimens are also reported in Table 5. Without hydrogen the fracture surfaces of S355 (Fig. 4.a) and H8 (Fig. 4.c) steels have the typical ductile appearance, characterized by the nucleation, growth and coalescence of microvoids (MVC). The WM steel (Fig. 4.e) shows a predominantly brittle cleavage (C) fracture and some areas with small dimples can also be seen in the image. When internal hydrogen is present, the morphology of the failure surfaces changes. The fracture surface of the S355 steel maintains a ductile appearance and the effect of hydrogen is only noticeable on the general aspect of microvoids, which are bigger and flatter in this case (this feature is related with the action of a hydrogen-enhanced localised plasticity mechanism, HELP). When hydrogen is present in the WM steel, intergranular features appear, mixed with a general cleavage micromechanism (Fig. 4.f), aspects in this case related to the action of a hydrogen-enhanced decohesion embrittlement micromechanism (HEDE). Finally, the presence of hydrogen in the H8 steel completely modifies its fracture behaviour, from ductile to brittle, with typical cleavage features appearing (Fig. 4.d). H8 steel has the highest HEI and the most radical change in the operative fracture micromechanism.

From the same fracture toughness tests, the evolution of the crack tip opening displacement parameter with the growth of the crack was also calculated, obtaining the *CTOD* $-R(\delta - R)$ curves. Values of δ were obtained following [46], using the following expression:

$$\delta = \delta_{el} + \delta_p = \frac{K_I^2}{m\sigma_{YS}E} + \frac{r_p(W-a)v_p}{r_p(W-a)+a} \tag{4}$$

where K_I is the stress intensity factor, E is Young's Modulus, r_p is the plastic rotational factor ($r_p = 0.44$), v_p is the displacement of the plastic part of the clip gauge opening and m is a parameter that depends on the specimen geometry (m = 2 for the tested geometry). The values of the critical CTOD parameter, δ_{Ic} (also defined for a stable crack growth of 0.2 mm) are show in Table 6. This table also shows the HEI obtained when CTOD is taken as a fracture parameter. The HEI obtained with pre-charged hydrogen gas associated with δ_{Ic} is low for S355 steel, very high for H8, and has an intermediate value for the WM steel.

3.2. Small Punch Tests on notched specimens

Small Punch Tests (SPTs) were carried out using the standard SPT device but on notched specimens. The standard device consists of a hemispherical-head punch with a diameter of 2.5 mm, a lower die hole with a diameter of 4 mm and a 0.2 mm chamfer edge (Fig. 5a). In order to increase hydrogen embrittlement (increasing the triaxiality of the sample), a longitudinal non-through thickness notch,

Table 4
Permeation tests results.

Parameter	Steel		
	S355	H8	WM
$D_{eff}\left(\text{x}10^{-11}m^2/s\right)$	130	8.5	1.1

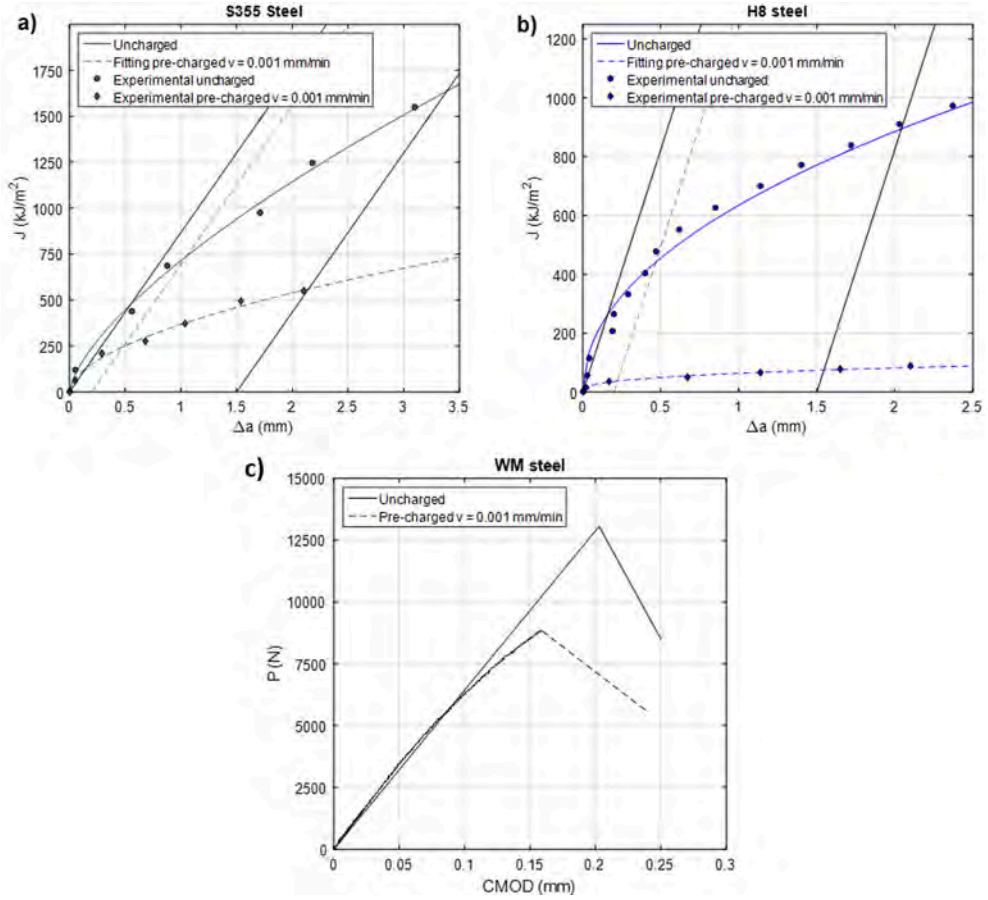

Fig. 3. Fracture toughness tests curves without internal hydrogen and pre-charged with hydrogen gas: a) S355 b) H8 c) WM.

Table 5
Results of the standard fracture toughness tests: J_{IC} and HEI values.

Material	As received		Pre-charged in hydrogen gas		HEI (%)
	J_{Ic}(kJ/m^2)	Failure micromechanisms[1]	$J_{Ic(H)}$(kJ/m^2)	Failure micromechanisms[1]	
S355	750 ± 20	MVC	247 ± 14	MVC	67
H8	450 ± 15	MVC	40 ± 18	C	91
WM	22 ± 5[2]	C	8 ± 3[2]	IG	64

[1] MVC: Microvoids coalescence, C: Cleavage, IG: Intergranular.
[2] Calculated using $J_{IC} = K_{IC}^2 \hat{A} \cdot (1-\nu^2)/E$.

with a depth-to-thickness relation $a/t = 0.3$ [21,47,48], was machined on the square SPT specimens, which had a mean thickness of 0.5 mm (10 × 10 × 0.5 mm, see Fig. 5.b). The load was applied using a mechanical testing machine equipped with a load cell with 5 kN of capacity and the punch displacement was measured with a *COD* extensometer. All the tests were performed in laboratory conditions at RT. Hydrogen-free SPT samples were tested using a standard test rate of 0.2 mm/min [49], but hydrogen pre-charged specimens were tested at a 10 times slower rate (0.02 mm/min) to allow the diffusion of hydrogen to the notch region during the tests and to maximize the possible embrittlement. At the end of the tests, the fracture SPT energy, W_{SPT}, was calculated as the area under the SPT curves up to the maximum load (Fig. 5b).

As well as the fracture energy, the SPT CTOD (δ_{SPT}) was also obtained using the procedure described in detail in Álvarez et al. [50]. Since it is not possible to measure this parameter directly when the test is in progress, some tests were interrupted for this specific purpose. Tests were interrupted around the maximum load (Fig. 6) and the width of the notch (Δ_F in Fig. 5a) was measured in a scanning electron microscope (SEM). The difference between the initial, Δ_I, and the final, Δ_F, notch widths (Fig. 5a), was δ_{SPT} (Eq. (5)) [50].

$$\delta_{SPT} = \Delta_F - \Delta_I \tag{5}$$

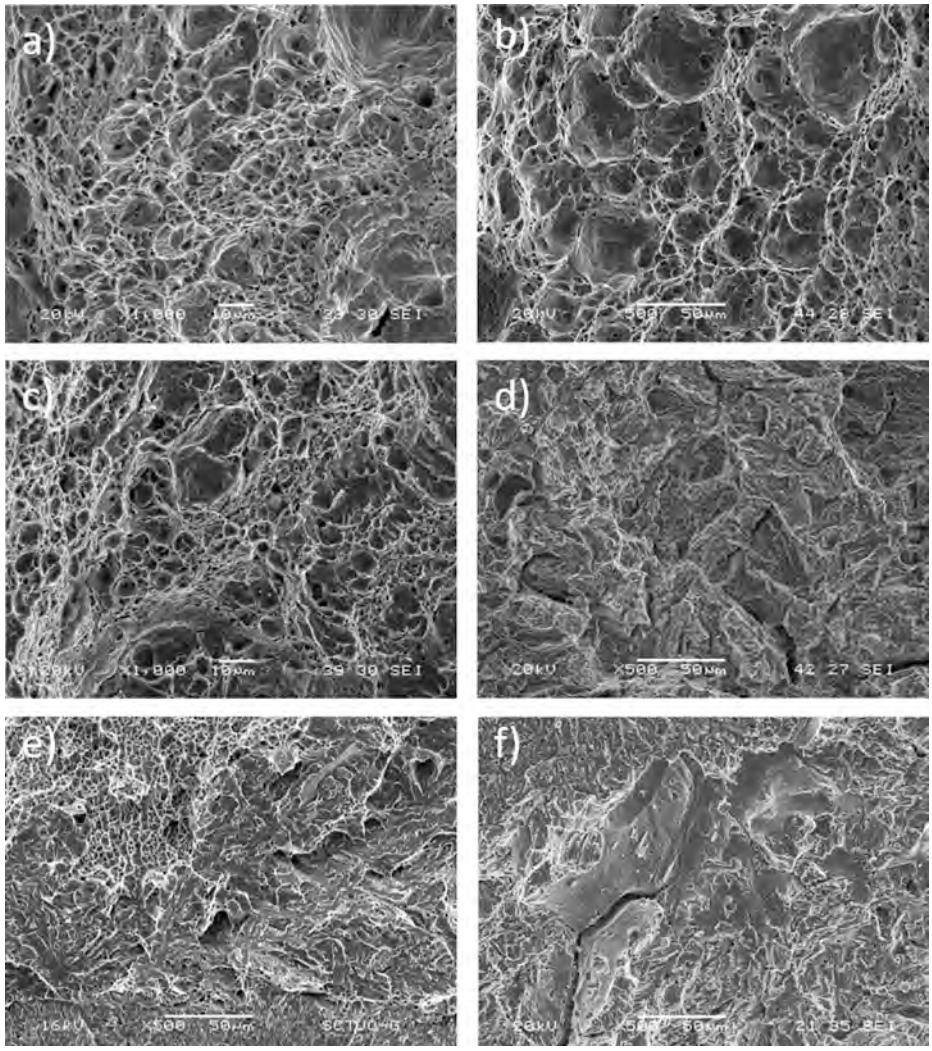

Fig. 4. Failure surfaces of SENB specimens. a) S355 without hydrogen; b) S355 H-pre-charged; c) H8 without hydrogen; d) H8 H-pre-charged; e) WM without hydrogen; f) WM H-pre-charged;

Table 6
Standard fracture toughness test, CTOD values for the initiation of crack growth.

Material	δ_{Ic}(mm)	$\delta_{Ic(H)}$(mm)	HEI (%)
S355	0.480	0.400	17
H8	0.240	0.040	83
WM	0.008	0.004	50

Fig. 6 shows the SPT curves obtained with the three steels without hydrogen and with internal hydrogen using the gaseous and cathodic pre-charging methods (between three and five samples were tested per each material and condition). The fracture SPT energy, W_{SPT}, derived from these curves, was divided by the square of the sample thickness to calculate the energy per unit of area. The corresponding HEI values were also determined using W_{SPT}/t^2 as a fracture parameter. These results are summarized in Table 7. The WM steel was the most embrittled steel, showing a HEI of 60.4% under gaseous pre-charged hydrogen and reaching 81.3% with cathodic pre-charging. The other two analysed steels had negligible embrittlement, especially after gaseous hydrogen pre-charging.

As in the standard test, a fractographic analysis was performed on the failed SPT specimens. The three steels exhibited fully ductile failure surfaces in the tests performed without hydrogen. In this case the low triaxiality in the region close to the SPT notch was not able to trigger brittle fracture micromechanisms, even in the WM steel. When internal hydrogen is present (both gaseous and cathodic), the failure mode of S355 (Fig. 7.a) and H8 (Fig. 7.b) did not change, remaining ductile. However, in the case of the WM steel, a general brittle appearance (cleavage) with radial cracks is visible (Fig. 7.c).

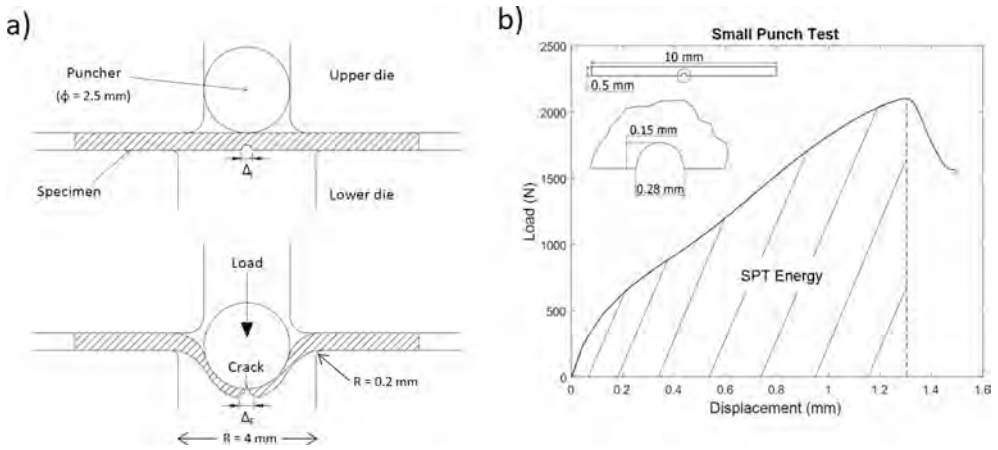

Fig. 5. SPT test. a) Notched SPT sample and loading; b) SPT curve and SPT energy determination.

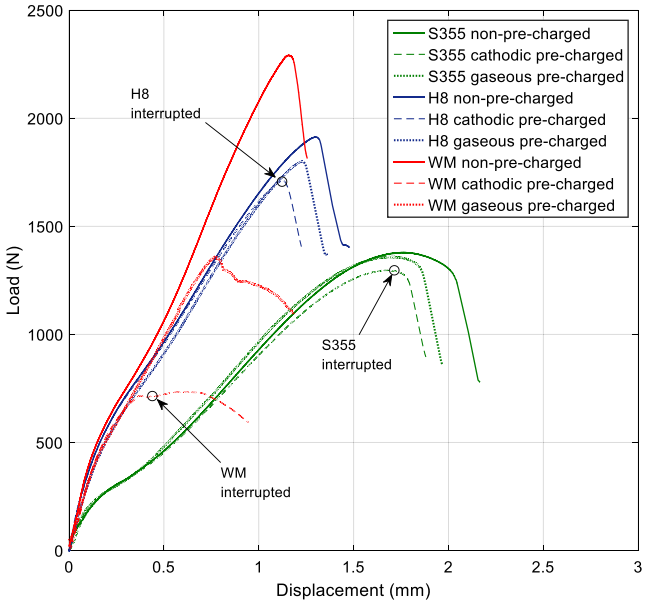

Fig. 6. Load - displacement SPT curves.

Table 7
SPT results: W_{SPT}/t^2 and HEI values.

Material	Ambient	Gaseous		Cathodic	
	$W_{SPT}/t^2(kJ/mm^2)$	$W^{gaseous}_{SPT(H)}/t^2(kJ/mm^2)$	HEI (%)	$W^{cathodic}_{SPT(H)}/t^2(kJ/mm^2)$	HEI (%)
S355	11049 ± 301	10850 ± 569	1.8 ± 3.2	10080 ± 178	8.8 ± 1.6
H8	10784 ± 588	10220 ± 421	5.2 ± 4.3	8702 ± 489	19.3 ± 4.5
WM	7140 ± 180	2832 ± 211	60.4 ± 2.9	1334 ± 211	81.3 ± 2.6

Because the hydrogen gas pre-charge had a minimum effect on the embrittlement analysis using the δ_{SPT} parameter, and because it required the test to be interrupted in order to measure the notch opening, testing was only carried out using cathodic pre-charged samples. The δ_{SPT} and HEI values obtained in these tests with each steel are reported in Table 8. As can be seen, S355 and H8 steels suffered no embrittlement under internal hydrogen when we use δ_{SPT} as a fracture parameter, and the HEI of WM steel only reaches 3%.

In the notch region of the hydrogen pre-charged SPT tests interrupted at the maximum load, long cracks growing along the notch length are clearly visible (Fig. 8). They are always located close to the middle of the notch length (region submitted to maximum

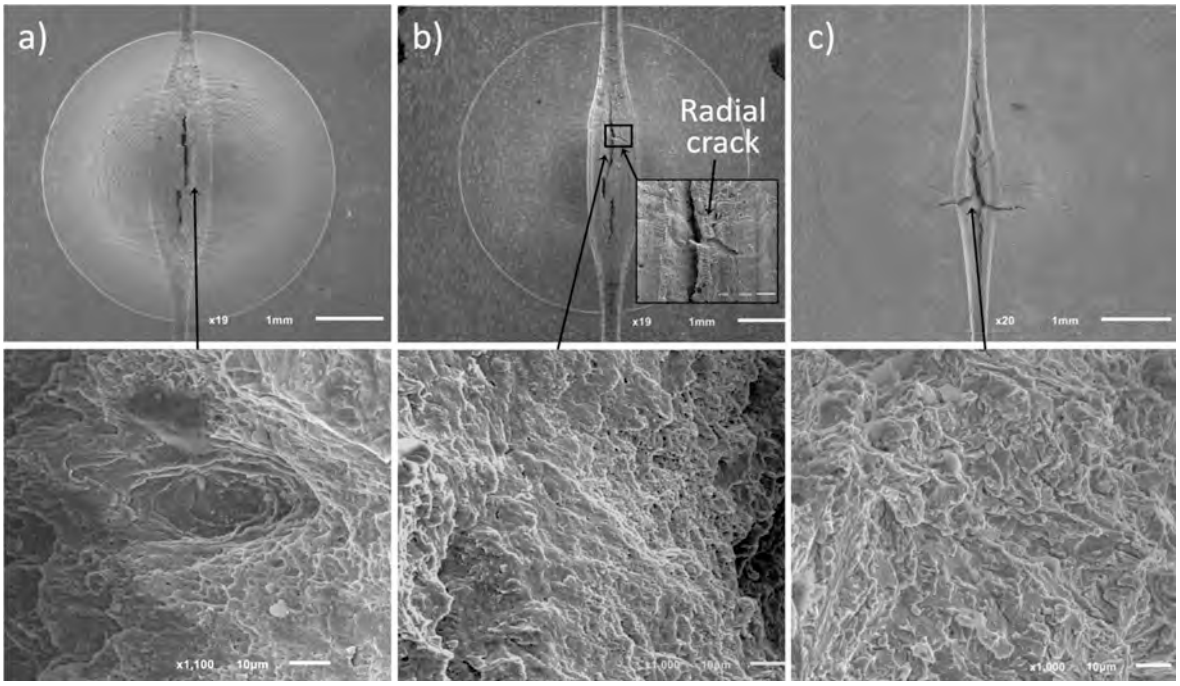

Fig. 7. SPT - cathodic pre-charging fractographies; a) S355 Hydrogen pre-charged general view; b) H8 Hydrogen pre-charged surface; c) WM Hydrogen pre-charged general view.

Table 8
Experimental δ_{SPT} results.

	δ_{SPT}^{air}(mm)	$\delta_{SPT(H)}^{cathodic}$(mm)	HEI (%)
S355	0.387	0.391	0
H8	0.377	0.379	0
WM	0.270	0.263	3

stresses). In the non-charged specimens cracks appear next to the maximum plastic strain zones [33]. Cracks are much more evident on the WM steel, in which intergranular cracking can also be seen in the enlarged image.

4. Discussion

The embrittlement of three structural steels using standard fracture toughness and Small Punch Tests was analysed and different values on the embrittlement indexes were obtained. Two hydrogen pre-charged methods were applied to the SPT samples and the gaseous pre-charge technique produced significantly lower values on the HEI than with cathodic charging. Various reasons explain these results.

Although a high quantity of hydrogen is introduced in the steels in the high pressure, high temperature gaseous pre-charge used in this work [43], a cooling phase of about 1 h (from 450 °C to 80 °C) is necessary before extracting the samples from the hydrogen reactor. During this time large hydrogen losses occur. This fact explains the relatively low hydrogen content measured after gaseous pre-charging (Table 3).

Regardless of the pre-charging method, the size of the sample and the hydrogen diffusion coefficient of the steel influences the amount of internal hydrogen present at the moment when the mechanical test starts. This fact could explain the different HEI results shown in the tests.

Knowing the values of C_{H0}(Table3)andD_{eff} (Table 4), it is possible to estimate the variation with time of the hydrogen concentration at any point of the thickness of the specimen, x, using Fick's second law (Expression (6)):

$$C(x,t) = C_{H0}\hat{A} \cdot \mathrm{erf}\left(\frac{x}{2\sqrt{D_{eff}t}}\right)$$

Applying Expression 6, Fig. 9 a) shows the evolution of hydrogen concentration at mid-thickness estimated for the three steels in the two specimen geometries (x = 0.25 mm for SPT and x = 3.75 mm for standard fracture toughness specimens). As can be seen, the

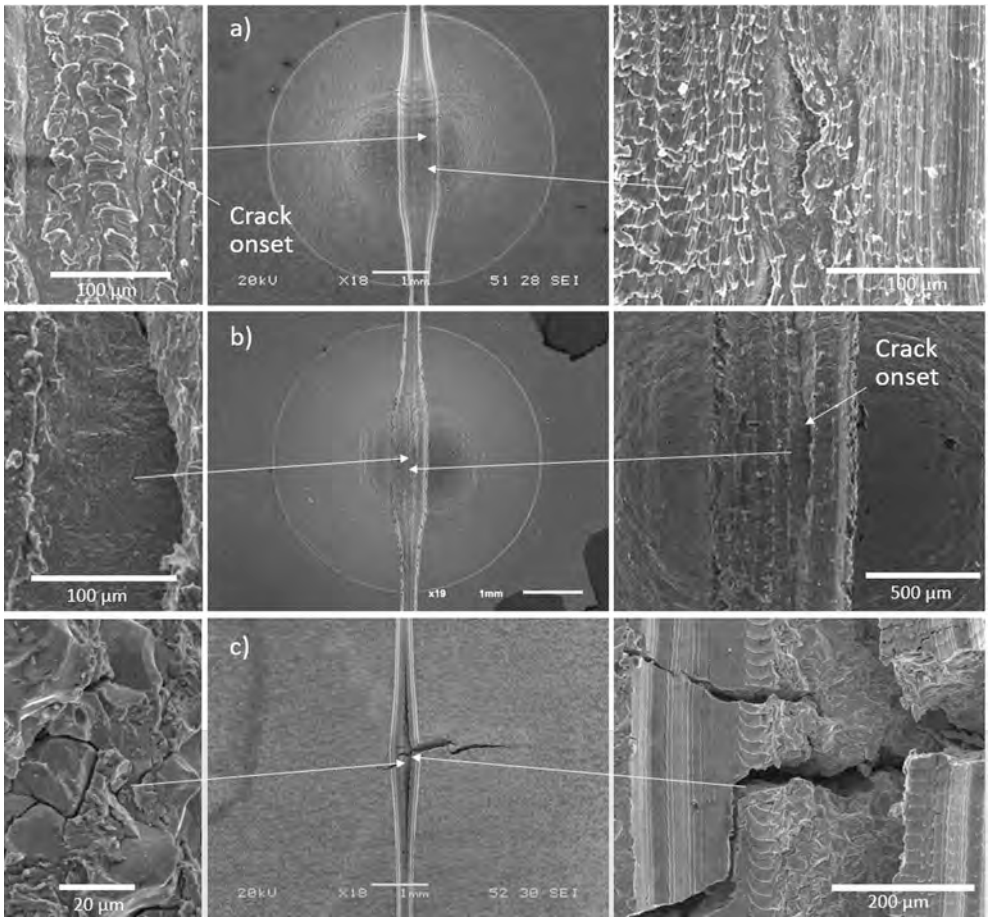

Fig. 8. Cathodically pre-charged SPT interrupted at maximum load with enlargements of the area of interest; a) S355; b) H8; c) WM.

SPT specimens (continuous lines), especially the S355 steel (green line) lose a large quantity of hydrogen in the first 300 s after the pre-charge conclusion. This is the time necessary to prepare the SPT test: to clean and mount the sample in the testing device and start the test. It was expected that a significant amount of hydrogen would diffuse out of the sample during this time (between 0 and 25% in function of the steel diffusion coefficient). Large hydrogen losses also take place in the course of these SPT tests. However, the standard fracture toughness specimens (triangles in Fig. 9.a) have almost 100% of the initial concentration of hydrogen in the middle of the sample thickness at the start of the test (approximately 1800 s, after their extraction from the liquid nitrogen Dewar). It is therefore concluded that the test preparation time as well as the steel hydrogen diffusion coefficient are key factors in the test results.

Fig. 9 b) shows the hydrogen concentration through the specimen thickness at the start of the tests. The thickness ratio is expressed as depth divided by the specimen thickness. While the standard fracture toughness samples have almost 100% hydrogen in more than 80% of their volume, the thin SPT specimens, show a much lower concentration, especially the S355, which barely reaches 20% of hydrogen concentration at mid-thickness. So, using the same pre-charging method, the lower hydrogen concentration in the SPT specimens during the test can explain the lower hydrogen embrittlement measured with these tests. Only the WM SPT samples maintained quite high hydrogen levels, explaining the relatively high embrittlement indexes measured with this steel in this particular miniature test (Table 7).

In addition, the lower hydrogen embrittlement obtained with the SPT specimens can be explained by the lower triaxiality produced in these tests compared to the standard fracture toughness tests. It is known that hydrogen concentration accumulates in the crack front region where the hydrostatic stress, σ_H, attains maximum values. The SEN(B) specimens have a σ_H value of approximately 2.5times the yield strength of the steel [19], while σ_H in the SPT tests only reaches1.1 times the yield strength [21]. In order to know the importance of σ_H, it is necessary to use Expression (7), which provides the equilibrium hydrogen concentration in the crack/notch front region, C_{Heq} [51].

$$C_{Heq} = C_{Hdif} \cdot e^{(\sigma_H V_H / RT)} \tag{7}$$

where V_H is the partial molar volume of hydrogen (2 10^{-6} m^3/mol H), R is the universal gas constant, and T is the temperature in Kelvin.

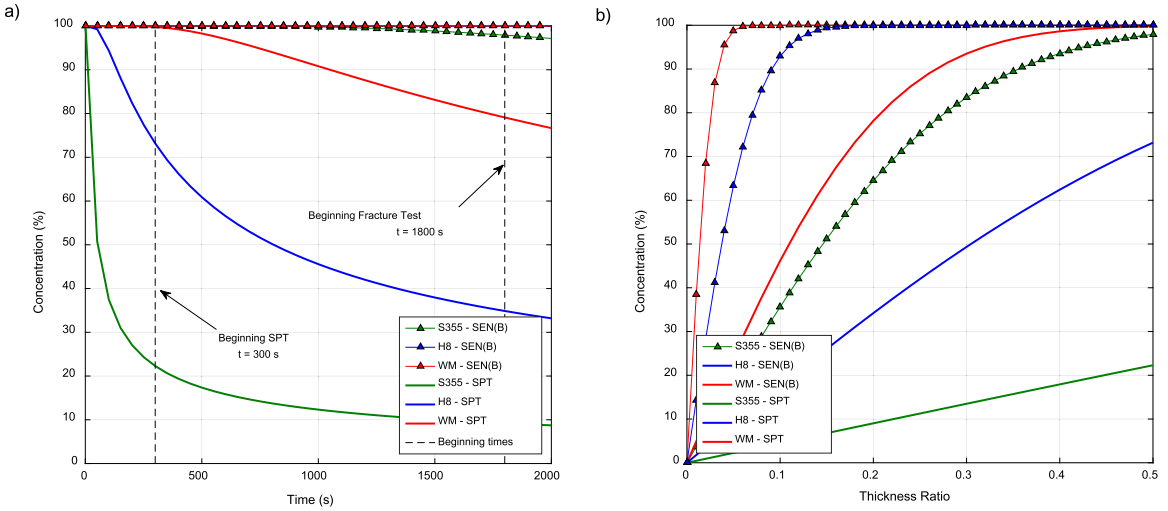

Fig. 9. a) Hydrogen concentration evolution in the middle of the specimen thickness, b) H evolution through the specimen thickness at the start of the tests.

Table 9 shows the results of applying Expression (7) to the different steels and specimen geometries taking into account the diffusible hydrogen values measured on the three steels after gaseous and cathodic pre-charging (Table 3). Hydrogen accumulation in the process zone (high hydrostatic stress) under gaseous pre-charging is much higher in the standard fracture toughness specimen than in the notched SPT test due to its higher triaxiality. However, as cathodic pre-charging introduces large hydrogen contents into the H8 and WM SPT samples, hydrogen accumulated in the process zone in the course of these low triaxiality tests may attain similar or even higher values than those estimated in the standard high triaxiality tests.

Another noteworthy point in this paper is the CTOD analysis. Table 6 shows a significant decrease in the CTOD values measured on the standard fracture toughness specimens, but the embrittlement effect is minimal in the notched SPT samples. The evolution of δ_{SPT} with the punch displacement in various metallic materials was analysed both numerically and experimentally in a previously published work [50] performed with identical SPT specimens and similar displacement rate (displacement rate differences between both set of tests do not modify results). In Fig. 10 the dashed lines represent the δ_{SPT} evolution from the beginning of the crack growth to the point where maximum load or displacement is reached and failure takes place. The continuous black line represents the theoretical response when damage is not taken into account in the numerical model. These values were obtained with non-hydrogenated samples of the three steels. Fig. 10 shows the experimental δ_{SPT} values measured at maximum load with individual points: shaded points for the cathodic pre-charged samples and empty points for the non-precharged samples. As can be seen, for the three tested steels, the obtained δ_{SPT} values are very similar regardless of whether the sample has internal hydrogen. However, the values of punch displacement corresponding to these δ_{SPT} results decreases when internal hydrogen is present. The measurements are taken at the point of maximum load, as seen in Fig. 6. However, this displacement decrease depends on the steel tested. H8 and S355 steels have a very low change in the SPT displacement at failure, so hydrogen has a minimal effect on this parameter. However, for WM, very different results were obtained in tests performed with and without hydrogen. When hydrogen is present, the onset of the crack growth occurs much earlier. Large cracks were observed in the notch region of S355 and H8 steels interrupted at maximum load and even more evident cracking was detected in the corresponding WM samples (Fig. 8), confirming that crack initiation takes place before reaching the maximum load in this test. Based on these results, it is possible to say that SPT is a good option to detect hydrogen embrittlement through the measurement of the SPT energy at failure. However, the use of δ_{SPT} as a fracture parameter is not recommended, because crack growth initiates before the maximum load (where it is usually supposed crack initiates), and the onset of crack growth in these tests is not properly defined.

Table 9
Hydrogen content in the process zone, C_{Heq}, for the different geometries and steels

Material	Standard fracture toughness test	Small Punch Test	
	Gaseous	Gaseous	Cathodic
S355	0.40	0.26	0.14
H8	3.62	1.44	3.30
WM	9.15	2.79	10.67

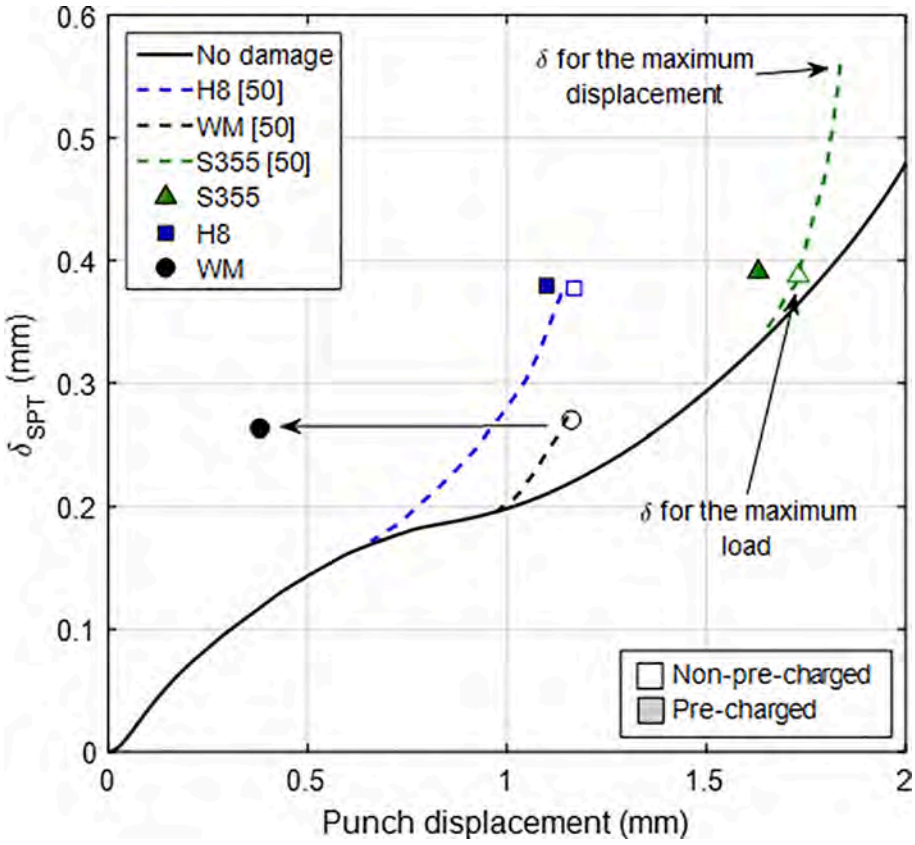

Fig. 10. δ_{SPT}- Punch displacement.

5. Conclusions

Two types of tests were used in this work: standard fracture toughness and the Small Punch Test (SPT). In addition, two pre-charging methods were used to introduce hydrogen into the samples. In both cases, energetic (J and W_{SPT}), and crack tip displacement (CTOD and δ_{SPT}) criteria, along with SEM observations were used to determine hydrogen embrittlement.

First at all, the influence of the steel microstructure on the hydrogen diffusion coefficient was analysed. This coefficient decreases as the strength of the steel increases. In this respect, hydrogen diffusion is critical in thin specimens, where the time between pre-charging and the start of the mechanical test is a key issue. Cathodic pre-charging is therefore recommended when thin specimens, such as SPT samples, are used. Thermal charging with high pressure, high temperature H_2 gas is only a good option for thick specimens, as significant hydrogen losses take place during sample cleaning and mounting in the testing device when SPT samples are used.

The effect of stress concentrators was also studied. The hydrostatic stress in the process zone was significantly lower in the SPT samples than in the standard fracture toughness specimen. Using cathodic pre-charging, high levels of diffusible hydrogen can be introduced into the SPT samples, giving hydrogen contents in the area in front of the notch similar to those in the process zone of the standard fracture toughness specimens. The low triaxiality of the SPT explains the lower hydrogen embrittlement indexes obtained in these mechanical tests.

Using both mechanical tests and fractographic analysis, it has been observed that the value of the HEI of the samples increases greatly when there is a change in fracture behaviour from ductile to brittle. This change was observed in both cases (with the standard test for the H8 and with the SPT for the WM). Using the standard fracture test and the CTOD evaluation, a decrease in the HEI was observed. However, when using the SPT this decrease was not observed.

The use of δ_{SPT} as a fracture parameter is not recommended, when it is defined at the maximum load registered in the SPT load–displacement curve. This is because crack growth initiates before that load, so the onset of crack growth in these tests cannot be properly defined in this way. However, the fracture SPT energy, W_{SPT}, derived from SPT load–displacement curves can be used as a valuable toughness parameter to characterize hydrogen embrittlement in steels, although it cannot replace the use of fracture standard tests on pre-cracked specimens due to constraint differences between both type of samples.

6. Data availability

The raw/processed data required to reproduce these findings cannot be shared at this time as the data also forms part of an ongoing

study

Declaration of Competing Interest

The authors declare that they have no known competing financial interests or personal relationships that could have appeared to influence the work reported in this paper.

Acknowledgement

Funding: This work was supported by the Spanish Ministry of Science, Innovation and Universities RTI2018-096070-B-C31. The authors G. Álvarez and A. Zafra would like to thank the Principality of Asturias for the support received with the Severo Ochoa grants, PA-20-PF-BP19-087 and PA-18-PF-BP17-038 respectively.

Finally, the authors also thank the Scientific and Technical Service, University of Oviedo, for the use of the SEM JEOL-JSM5600 scanning electron microscope.

References

[1] Dincer I, Acar C. Smart energy solutions with hydrogen options. Int J Hydrogen Energy 2018;43(18):8579–99. https://doi.org/10.1016/j.ijhydene.2018.03.120.
[2] Zhao W, Zhang T, Zhao Y, Sun J, Wang Y. Hydrogen permeation and embrittlement susceptibility of X80 welded joint under high-pressure coal gas environment. Corros Sci 2016;111:84–97. https://doi.org/10.1016/J.CORSCI.2016.04.029.
[3] Djukic MB, Sijacki Zeravcic V, Bakic GM, Sedmak A, Rajicic B. Hydrogen damage of steels: A case study and hydrogen embrittlement model. Eng Fail Anal 2015; 58:485–98. https://doi.org/10.1016/J.ENGFAILANAL.2015.05.017.
[4] Zafra A, Álvarez G, Belzunce J, Alegre JM, Rodríguez C. Fracture toughness of coarse-grain heat affected zone of quenched and tempered CrMo steels with internal hydrogen: Fracture micromechanisms. Eng Fract Mech 2021;241:107433. https://doi.org/10.1016/j.engfracmech.2020.107433.
[5] Zhang T, Zhao W, Li T, Zhao Y, Deng Q, Wang Y, et al. Comparison of hydrogen embrittlement susceptibility of three cathodic protected subsea pipeline steels from a point of view of hydrogen permeation. Corros Sci 2018;131:104–15. https://doi.org/10.1016/j.corsci.2017.11.013.
[6] Singh DK, Singh Raman RK, Maiti SK, Bhandakkar TK, Pal S. Investigation of role of alloy microstructure in hydrogen-assisted fracture of AISI 4340 steel using circumferentially notched cylindrical specimens. Mater Sci Eng A 2017;698:191–7. https://doi.org/10.1016/J.MSEA.2017.05.056.
[7] Hu Y, Dong C, Luo H, Xiao K, Zhong P, Li X. Study on the Hydrogen Embrittlement of Aermet100 Using Hydrogen Permeation and SSRT Techniques; n.d. https://doi.org/10.1007/s11661-017-4159-x.
[8] Fan YH, Zhang B, Yi HL, Hao GS, Sun YY, Wang JQ, et al. The role of reversed austenite in hydrogen embrittlement fracture of S41500 martensitic stainless steel. Acta Mater 2017;139:188–95. https://doi.org/10.1016/j.actamat.2017.08.011.
[9] Cheng L, Li L, Zhang X, Liu J, Wu K. Numerical simulation of hydrogen permeation in steels. Electrochim Acta 2018;270:77–86. https://doi.org/10.1016/J.ELECTACTA.2018.03.061.
[10] Misawa T, Suzuki K, Saito M, Hamaguchi Y. Determination of the minimum quantity of irradiated ferritic steel specimens for small punch DBTT testing. J Nucl Mater 1991;179–181:421–4. https://doi.org/10.1016/0022-3115(91)90114-M.
[11] García TE, Rodríguez C, Belzunce FJ, Peñuelas I, Arroyo B. Development of a methodology to study the hydrogen embrittlement of steels by means of the small punch test. Mater Sci Eng A 2015;626:342–51. https://doi.org/10.1016/j.msea.2014.12.083.
[12] García TE, Arroyo B, Rodríguez C, Belzunce FJ, Álvarez JA. Small punch test methodologies for the analysis of the hydrogen embrittlement of structural steels. Theor Appl Fract Mech 2016;86:89–100. https://doi.org/10.1016/J.TAFMEC.2016.09.005.
[13] Arroyo B, Álvarez JA, Lacalle R, Uribe C, García TE, Rodríguez C. Analysis of key factors of hydrogen environmental assisted cracking evaluation by small punch test on medium and high strength steels. Mater Sci Eng A 2017;691:180–94. https://doi.org/10.1016/J.MSEA.2017.03.006.
[14] Guan K, Szpunar JA, Matocha K, Wang D. Study on temper embrittlement and hydrogen embrittlement of a hydrogenation reactor by small punch test. Materials (Basel) 2017;10:671. https://doi.org/10.3390/ma10060671.
[15] Nguyen TT, Park JS, Kim WS, Nahm SH, Beak UB. Environment hydrogen embrittlement of pipeline steel X70 under various gas mixture conditions with in situ small punch tests. Mater Sci Eng A 2020;781:139114. https://doi.org/10.1016/j.msea.2020.139114.
[16] Nambu T, Shimizu K, Matsumoto Y, Rong R, Watanabe N, Yukawa H, et al. Enhanced hydrogen embrittlement of Pd-coated niobium metal membrane detected by in situ small punch test under hydrogen permeation. J Alloys Compd 2007;446-447:588–92. https://doi.org/10.1016/j.jallcom.2007.02.063.
[17] Zafra A, Peral LB, Belzunce J, Rodríguez C. Effect of hydrogen on the tensile properties of 42CrMo4 steel quenched and tempered at different temperatures. Int J Hydrogen Energy 2018;43(18):9068–82. https://doi.org/10.1016/j.ijhydene.2018.03.158.
[18] Peral LB, Zafra A, Belzunce J, Rodríguez C. Effects of hydrogen on the fracture toughness of CrMo and CrMoV steels quenched and tempered at different temperatures. Int J Hydrogen Energy 2019;44(7):3953–65. https://doi.org/10.1016/j.ijhydene.2018.12.084.
[19] Álvarez G, Peral LB, Rodríguez C, García TE, Belzunce FJ. Hydrogen embrittlement of structural steels: Effect of the displacement rate on the fracture toughness of high-pressure hydrogen pre-charged samples. Int J Hydrogen Energy 2019;44(29):15634–43. https://doi.org/10.1016/j.ijhydene.2019.03.279.
[20] Cuesta II, Alegre JM, García TE, Rodríguez C. Influence of the notch shape of pre-notched small punch specimens on the creep failure time. Eng Fail Anal 2015; 56:332–7. https://doi.org/10.1016/j.engfailanal.2015.01.008.
[21] García TE, Rodríguez C, Belzunce FJ, Cuesta II. Development of a new methodology for estimating the CTOD of structural steels using the small punch test. Eng Fail Anal 2015;50:88–99. https://doi.org/10.1016/j.engfailanal.2015.01.011.
[22] Song EJ, Baek S-W, Nahm SH, Baek UB. Notched-tensile properties under high-pressure gaseous hydrogen: Comparison of pipeline steel X70 and austenitic stainless type 304L, 316L steels. Int J Hydrogen Energy 2017;42(12):8075–82. https://doi.org/10.1016/j.ijhydene.2016.12.069.
[23] Nanninga NE, Levy YS, Drexler ES, Condon RT, Stevenson AE, Slifka AJ. Comparison of hydrogen embrittlement in three pipeline steels in high pressure gaseous hydrogen environments. Corros Sci 2012;59:1–9. https://doi.org/10.1016/J.CORSCI.2012.01.028.
[24] Briottet L, Batisse R, de Dinechin G, Langlois P, Thiers L. Recommendations on X80 steel for the design of hydrogen gas transmission pipelines. Int J Hydrogen Energy 2012;37(11):9423–30. https://doi.org/10.1016/j.ijhydene.2012.02.009.
[25] Briottet L, Moro I, Escot M, Furtado J, Bortot P, Tamponi GM, et al. Fatigue crack initiation and growth in a CrMo steel under hydrogen pressure. Int J Hydrogen Energy 2015;40(47):17021–30. https://doi.org/10.1016/j.ijhydene.2015.05.080.
[26] Meng Bo, Gu C, Zhang L, Zhou C, Li X, Zhao Y, et al. Hydrogen effects on X80 pipeline steel in high-pressure natural gas/hydrogen mixtures. Int J Hydrogen Energy 2017;42(11):7404–12. https://doi.org/10.1016/j.ijhydene.2016.05.145.
[27] Michler T, Naumann J. Hydrogen embrittlement of Cr-Mn-N-austenitic stainless steels. Int J Hydrogen Energy 2010;35(3):1485–92. https://doi.org/10.1016/j.ijhydene.2009.10.050.
[28] Colombo C, Fumagalli G, Bolzoni F, Gobbi G, Vergani L. Fatigue behavior of hydrogen pre-charged low alloy Cr–Mo steel. Int J Fatigue 2016;83:2–9. https://doi.org/10.1016/j.ijfatigue.2015.06.002.
[29] Alvaro A, Wan D, Olden V, Barnoush A. Hydrogen Enhanced Fatigue Crack Growth Rates in a Ferritic Fe-3wt%Si Alloy. Procedia Struct Integr 2018;13:1514–20. https://doi.org/10.1016/J.PROSTR.2018.12.310.

[30] Li X, Zhang J, Shen S, Wang Y, Song X. Effect of tempering temperature and inclusions on hydrogen-assisted fracture behaviors of a low alloy steel. Mater Sci Eng A 2017;682:359–69. https://doi.org/10.1016/j.msea.2016.11.064.
[31] Barnoush A, Vehoff H. Recent developments in the study of hydrogen embrittlement: Hydrogen effect on dislocation nucleation. Acta Mater 2010;58(16): 5274–85. https://doi.org/10.1016/j.actamat.2010.05.057.
[32] Simoni L, Caselani JQ, Ramos LB, Schroeder RM, Malfatti Cde F. The influence of calcareous deposits on hydrogen uptake and embrittlement of API 5CT P110 steel. Corros Sci 2017;118:178–89. https://doi.org/10.1016/J.CORSCI.2017.02.007.
[33] Depover T, Wallaert E, Verbeken K. Fractographic analysis of the role of hydrogen diffusion on the hydrogen embrittlement susceptibility of DP steel. Mater Sci Eng A 2016;649:201–8. https://doi.org/10.1016/J.MSEA.2015.09.124.
[34] Dadfarnia M, Sofronis P, Neeraj T. Hydrogen interaction with multiple traps: Can it be used to mitigate embrittlement? Int J Hydrogen Energy 2011;36(16): 10141–8. https://doi.org/10.1016/j.ijhydene.2011.05.027.
[35] Fernández-Sousa R, Betegón C, Martínez-Pañeda E. Analysis of the influence of microstructural traps on hydrogen assisted fatigue. Acta Mater 2020;199: 253–63. https://doi.org/10.1016/j.actamat.2020.08.030.
[36] Frappart S, Feaugas X, Creus J, Thebault F, Delattre L, Marchebois H. Study of the hydrogen diffusion and segregation into Fe–C–Mo martensitic HSLA steel using electrochemical permeation test. J Phys Chem Solids 2010;71(10):1467–79. https://doi.org/10.1016/j.jpcs.2010.07.017.
[37] Bueno AHS, Moreira ED, Gomes JACP. Evaluation of stress corrosion cracking and hydrogen embrittlement in an API grade steel. Eng Fail Anal 2014;36:423–31. https://doi.org/10.1016/J.ENGFAILANAL.2013.11.012.
[38] Zhao W, Zhang T, He Z, Sun J, Wang Y. Determination of the Critical Plastic Strain-Induced Stress of X80 Steel through an Electrochemical Hydrogen Permeation Method. Electrochim Acta 2016;214:336–44. https://doi.org/10.1016/J.ELECTACTA.2016.08.026.
[39] Bueno AHS, Moreira ED, Siqueira P, Gomes JACP. Effect of cathodic potential on hydrogen permeation of API grade steels in modified NS4 solution. Mater Sci Eng A 2014;597:117–21. https://doi.org/10.1016/J.MSEA.2013.12.033.
[40] Zafra A, Belzunce J, Rodríguez C. Hydrogen diffusion and trapping in 42CrMo4 quenched and tempered steel: Influence of quenching temperature and plastic deformation. Mater Chem Phys 2020;255:123599. https://doi.org/10.1016/j.matchemphys.2020.123599.
[41] UNE-EN 6892-1. Materiales metálicos Ensayo de tracción Parte 1 : Método de ensayo a temperatura ambiente; 2017.
[42] Álvarez G, Zafra A, Belzunce FJ, Rodríguez C. Hydrogen embrittlement analysis in a CrMoV steel by means of sent specimens. Theor Appl Fract Mech 2020;106: 102450. https://doi.org/10.1016/j.tafmec.2019.102450.
[43] Álvarez G, Zafra A, Rodríguez C, Belzunce FJ, Cuesta II. SPT analysis of hydrogen embrittlement in CrMoV welds. Theor Appl Fract Mech 2020;110:102813. https://doi.org/10.1016/j.tafmec.2020.102813.
[44] ASTM Standard G148 – 1997.Standard practice for evaluation of hydrogen uptake, permeation and transport in metals by an electrochemical technique 1997;i: 10. https://doi.org/10.1520/G0148-97R11.2.
[45] ASTM E 1820-01: Standard Test Method for Measurement of Fracture Toughness; 2001. https://doi.org/10.1520/E1820-09.2.
[46] Anderson TL. FRACTURE MECHANICS Fundamentals and Applications, Angew. Chemie Int. Ed. 2001. https://doi.org/10.1002/1521-3773(20010316)40: 6<9823::AID-ANIE9823>3.3.CO;2-C.
[47] Martínez-Pañeda E, García TE, Rodríguez C. Fracture toughness characterization through notched small punch test specimens. Mater Sci Eng A 2016;657: 422–30. https://doi.org/10.1016/j.msea.2016.01.077.
[48] Martínez-Pañeda E, Cuesta II, Peñuelas I, Díaz A, Alegre JM. Damage modeling in Small Punch Test specimens. Theor Appl Fract Mech 2016;86:51–60. https://doi.org/10.1016/J.TAFMEC.2016.09.002.
[49] Bruchhausen M, Austin T, Holmstrom S, Altstadt E, Dymacek P, Jeffs S, et al. European standard on small punch testing of metallic materials, 1A-2017; 2017. https://doi.org/10.1115/PVP2017-65396.
[50] Álvarez G, Rodríguez C, Belzunce FJ, García TE. Use of notched small punch test specimens for the determination of fracture properties in structural steels. Theor Appl Fract Mech 2020;106:102442. https://doi.org/10.1016/j.tafmec.2019.102442.
[51] Oriani RA. The diffusion and trapping of hydrogen in steel. Acta Metall 1970;18(1):147–57. https://doi.org/10.1016/0001-6160(70)90078-7.